Hydrology and
Earth System
Sciences
Discussions

# Early hypogene Carbonic Acid Speleogenesis in unconfined limestone aquifers by upwelling deep-seated waters with high $CO_2$ concentration: A first modelling approach

5  Franci Gabrovšek[1], Wolfgang Dreybrodt[1,2]

[1] Karst Research Institute ZRC SAZU, Titov trg 2, 6230 Postojna, Slovenia

[2] Faculty of Physics and Electrical Engineering, University of Bremen, Germany

*Correspondence to*: Franci Gabrovšek (gabrovsek@zrc-sazu.si)

**Abstract.** Hypogene caves originate from upwelling deep-seated waters loaded with $CO_2$ that mix with meteoric waters in a
10  limestone aquifer. Here we present first results on digital modelling of Carbonic Acid Speleogenesis (CAS). We study an
unconfined aquifer where meteoric water seeps through the vadose zone and becomes saturated with respect to calcite when
it arrives at the water table. From below deep-seated water with high $p_{CO_2}$ and saturated with respect to calcite invades the
limestone formation by forced flow. Two flow domains arise that host exclusively water from the meteoric or the deep-
seated source. They are separated by a water divide. There by dispersion of flow, a fringe of mixing arises and widening of
15  the fractures is caused by mixing corrosion (MC). The evolution of the cave system is determined by its early state. At sites
with high rates of fracture widening regions of higher hydraulic conductivity are created. They attract flow and support one
by one mixing with maximal dissolution rates. Therefore, the early evolution is determined by karstification originating close
to the input of the upwelling water and at the output at a seepaall ge face. In between these regions, a wide fringe of
moderate dissolution is present. In the later stage of evolution, this region is divided by constrictions that originate from
20  statistical variations of fracture aperture widths that favour high dissolution rates and focus flow into this region. This MC-
fringe-instability is an intrinsic property of cave evolution and is present in all scenarios studied. We have investigated the
influence of defined regions with higher fracture aperture widths. These determine the cave patterns and suppress MC-
fringe-instabilities. We have discussed the influence of the ratio of upwelling water flux rates to the rates of meteoric water.
This ratio specifies the position of the mixing fringe and consequently that of the cave system. In a further step, we have
25  explored the influence of time dependent meteoric recharge. Furthermore, we have modelled scenarios where waters are
undersaturated with respect to calcite. These findings give important insight into mechanisms of hypogene speleogenesis.
They also have implications to the understanding of sulfuric acid speleogenesis (SAS).

## 1 Introduction

Hydrochemical digital models of speleogenesis are powerful tools to understand the physical and chemical processes that

30  determine the evolution of caves. Initial models of the evolution of 1D fractures (Dreybrodt, 1990;Palmer, 1991) were soon extended to different manifestations of fracture networks within 2D and 3D domains (Groves and Howard, 1994;Siemers and Dreybrodt, 1998;Kaufmann et al., 2010;Li et al., 2020). Variety of hypothetical hydrological, structural and geochemical settings were envisioned in order to understand the basic speleogenetic mechanisms (Dreybrodt et al., 2005;Gabrovsek and Dreybrodt, 2010;Kaufmann, 2003;Birk et al., 2003). The models have also been used for a process-based interpretation of

35  real situations (Kaufmann and Romanov, 2019). The development of the models has been guided by theoretical insights based on small scale detailed studies of dissolution front propagation and fingering (Hanna and Rajaram, 1998;Cheung and Rajaram, 2002;Szymczak and Ladd, 2009;Dreybrodt and Gabrovšek, 2019). Most of the models simulate epigene speleogenesis governed by the aggressive solution from the surface.

Hypogene caves are defined by Palmer (2000;2007) from the geochemical view as "*those formed by water in which the*

40  *aggressiveness has been produced at depth beneath the surface, independent of surface or soil $CO_2$ or other near-surface acid sources.*" or by Klimchouk from a hydrological approach as "*the formation of solution-enlarged permeability structures (void-conduit systems) by fluids that recharge the cavernous zone from below, driven by hydrostatic pressure or other sources of energy, independent of direct recharge from the overlying or immediately adjacent surface*" (Klimchouk, 2007;Klimchouk, 2016).

45  Several modelling studies focused to speleogenesis along deep-flow pathways, which to some extend meet the criteria defined above (Rajaram et al., 2009;Chaudhuri et al., 2013;Kaufmann et al., 2014), but mostly focus to the temperature effect on flow and dissolution.

In the last decade hypogene caves have attracted broad interest in the karst community highlighting in the recent book" Hypogene Karst regions and caves of the world" (Klimchouk et al., 2017). The book gives a wide overview of hypogene

50  caves worldwide. Modelling efforts to this wealth of information are not reported. In this work we take a first step to explore by digital modelling the processes governing the initial evolution of hypogene caves.

There are various agents active in hypogene speleogenesis:

A) Dissolution by sulfuric acid (Palmer, 2013) occurs close to the surface where $H_2S$ bearing deep- seated waters rise from

55  below and mix with oxygenated shallow groundwater. There $H_2S$ is oxidized to sulfuric acid that dissolves limestone, releasing $CO_2$ for further dissolution of carbonate rock. This speleogenetic process, termed sulfuric acid speleogenesis, (SAS) has created large caves, e.g. Carlsbad Caverns in the Guadalupe reef complex in the United States and Frasassi cave system in Central Italy.

B) Another agent is carbonic acid, dominating epigene carbonate speleogenesis. It operates also as a hypogene agent that is

60  produced at depth, e. g. by thermal decomposition of carbonate rocks. This way $CO_2$ containing water with high $p_{CO2}$ to 1

Hydrology and
Earth System
Sciences
Discussions

atm can intrude into upper aquifers, especially in areas of young volcanism, point-wise or disperse, depending on geologic/structural conditions (Audra and Palmer, 2015;Klimchouk, 2013;Palmer, 2007;Jeong et al., 2005). $CO_2$ may also stem from oxidation of deep-seated organic compounds, as they are abundant near hydrocarbon fields (Klimchouk, 2019). In this work, we focus to hypogene carbonic acid speleogenesis (CAS) and from the results, we will discuss the problems that

65    arise in modelling of SAS.


## 2. The model

### 2.1. Modelling domain of an unconfined aquifer with mixing of surface and deep-seated waters

As the first step, we discuss the modelling domains and settings that determine hypogene karstification. Figure 1 shows the settings of an unconfined aquifer. A net of fracture conjunctions as depicted in a) each 2 m long and 1 m wide are connected

70    to form a rectangular array that presents a vertical 2D section of an unconfined aquifer of a selected depth and length. To each fracture, individually a selected aperture width is assigned.  This way a net with a lognormal distribution of aperture widths, as shown in b) is created. The following boundary conditions are applied: At the top of the domain, we impose a constant input, q, of water to each fracture to simulate the recharge by meteoric water. To each input fracture, a defined Ca-concentration and $p_{CO2}$ of the inflowing water is assigned.

75    At the left hand side, we impose no flow condition to model a water divide. The right hand side presents the outflow of water where each fracture is open to the atmosphere in the upper part (seepage face. The lower region is at no flow condition. Therefore, a water table arises that divides the aquifer into a vadose (light grey) and a phreatic zone (dark grey). The bottom boundary of the modelling domain is regarded impermeable (no flow condition, red) with the exception of a defined region (blue) where waters from the depth with defined chemical composition invade the aquifer with constant flow, Q,  into each

80    fracture. For each fracture where water enters into the aquifer, Ca-concentration and $p_{CO2}$ are selected.  In a pure $CaCO_3$-$CO_2$-$H_2O$ solution, these two parameters define all its chemical properties.
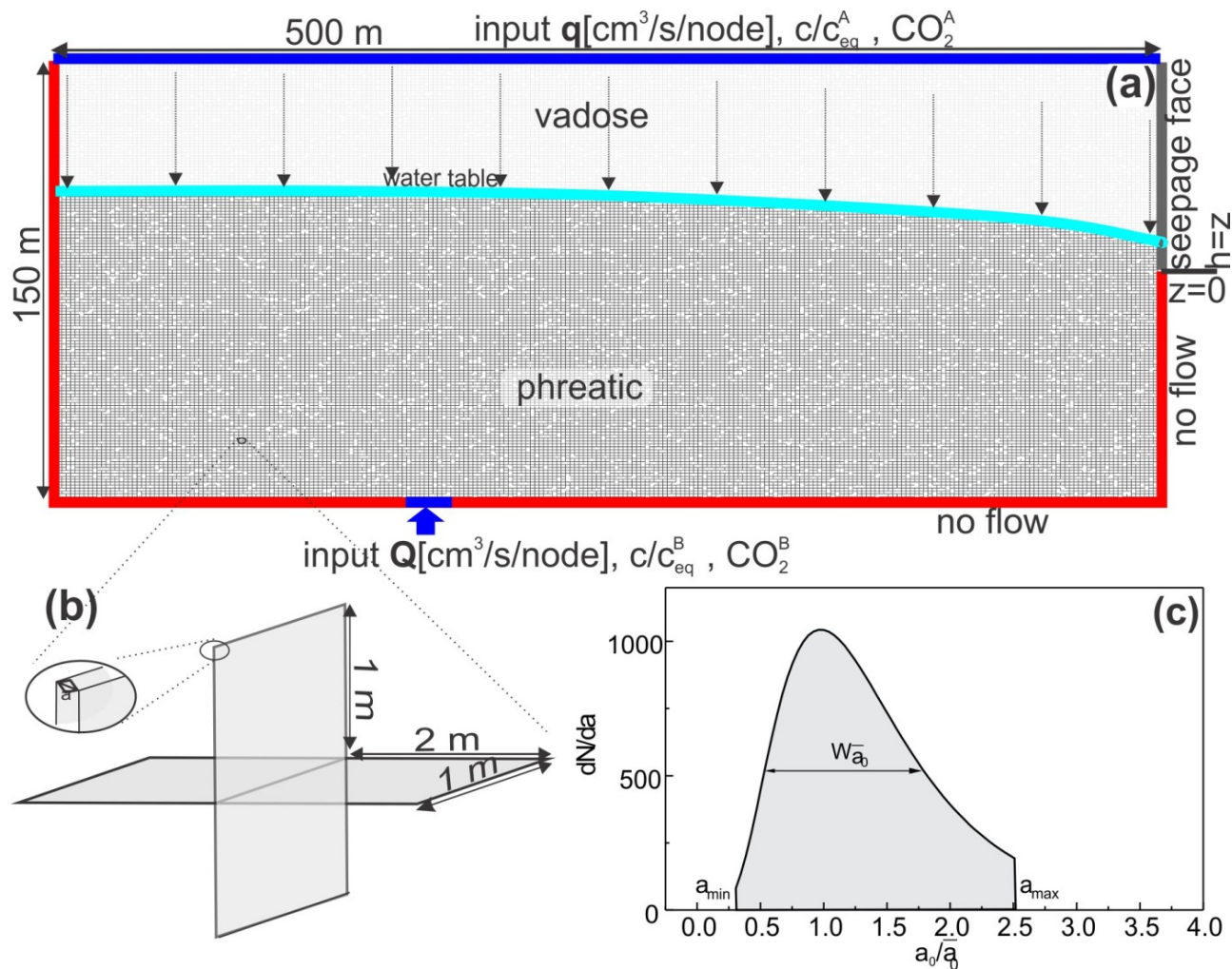
Figure 1: a) 2 dimensional fracture network presenting a vertical cross-section through unconfined aquifer. The length of the domain is 500 m, the depth is 150 m. Fracture spacing is $2 \times 1$ m$^2$ as depicted in b). Input q, cm$^3$/(s node) at the top is evenly distributed meteoric water percolating to the water table. When it arrives there, it has become saturated with respect to calcite and $p_{CO2}$. At the bottom of the domain deep-seated upwelling water enters with prescribed flow Q, cm$^3$/(s node) by forced flow. Due to dissolution of limestone on its way from below this water is saturated with respect to calcite and high $p_{CO2}$. The water flows to a seepage face located above height z = 0. Red border denotes no flow conditions, blue border denotes input of prescribed flow. Each fracture has an initial aperture width $a$, which is selected from a truncated log-normal distribution, shown in (c).

95   There is an important general property of flow under such boundary conditions. Whenever Darcy flow originates from different recharging sources, in our case, meteoric water to the water table and upwelling deep water from below, each source creates a flow domain that hosts only water originating from the corresponding recharge source. Flow domains of different origin of waters are separated by a water divide. The waters of differing origin do not mix. Only at the water divide mixing is possible caused by dispersion of flow into the fractures close to the water divide.

100   Fig. 2 presents an illustration. Water entering from below with equilibrium concentration $c_{eq}^{B}$ is coloured in red whereas recharge from the top with equilibrium concentration $c_{eq}^{a}$ is coloured in blue. Clearly two flow domains are visible. Water entering from below occupies the lower red region expanding from its input to the outflow at the seepage face. Water from the top (red) that recharges at the seepage face floats on the flow domain below. At the border between the two domains a fringe with rainbow colours is visible that indicate the mixing zone. The colours symbolize the equilibrium concentrations of

105 the mixed solutions and therefore also the mixing ratio as depicted by the colour code. Red is $V_A/V_B = 0/1$, green, $V_A/V_B = 1/1$, dark blue, $V_A/V_B = 1/0$.

The position of this mixing zone depends on the input ratio $q/Q$. With increasing ratio, the mixing zone shifts downwards. Therefore, at a constant inflow from below but varying recharge of meteoric water as it occurs likely during the evolution of caves, the mixing zone fluctuates up and down. When the water entering into the limestone aquifer is undersaturated with

110 respect to calcite we find two regions of limestone dissolution. Each of them extends from the input into the corresponding flow domains but stays limited there. There is also dissolution in the mixing zone where waters that have become saturated mix. However, even in the case when the input waters are saturated with respect to calcite mixing corrosion (MC) is active in the mixing fringe.
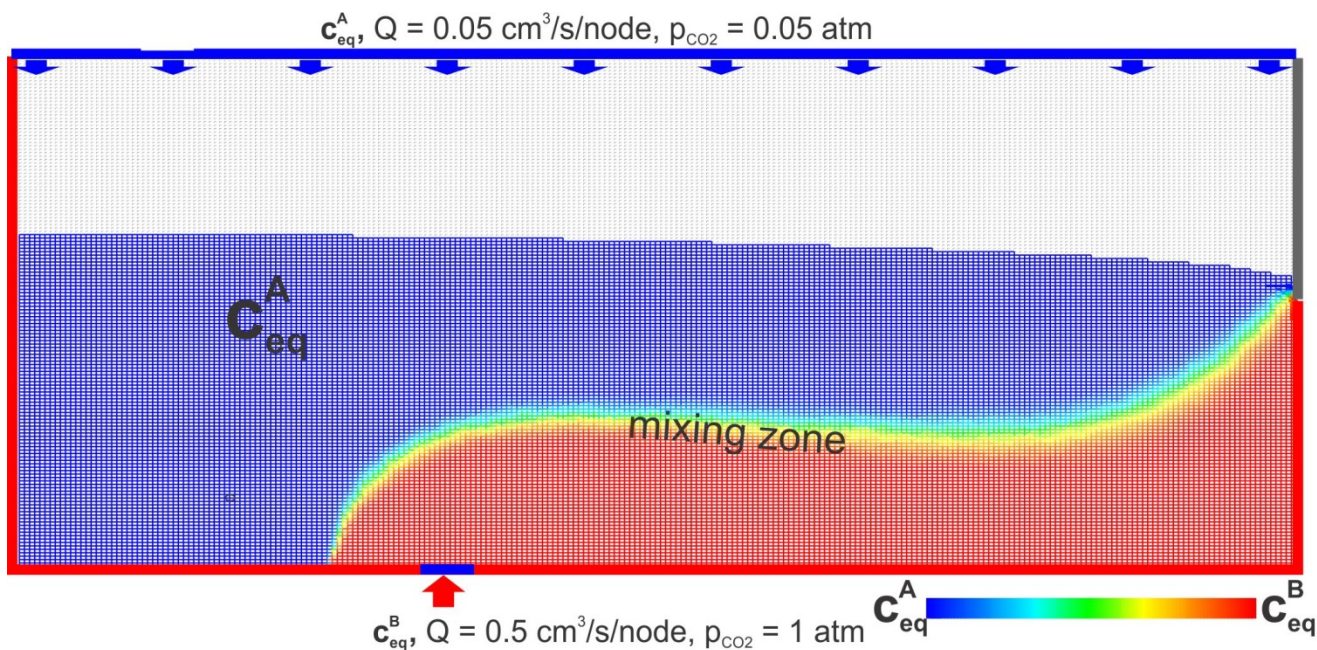
Figure 2: Visualization of the mixing zone. Two types of waters, one with calcium equilibrium concentration $c_{eq}^{B}$, and the other with equilibrium concentration, $c_{eq}^{b}$ invade the aquifer. Flow domains, red and blue are separated by a water divide. There dispersive mixing takes place and the equilibrium concentration of the mixed solution is between the values $c_{eq}^{B}$ and $c_{eq}^{A}$ (see Fig. 3). This is depicted by a colour code with red for the highest concentration $c_{eq}^{B}$ decreasing down through the optical spectrum to dark blue for concentration $c_{eq}^{A}$. This way the colours indicate the degree of mixing. The green region hosts one by one mixing.

## 2.2. The digital model

All information concerning the numerical scheme and the model is reported in previous literature: Details of the digital model are given by Dreybrodt et al. (2005), Gabrovšek and Dreybrodt (2010) and Dreybrodt and Gabrovšek (2019).The extension to unconfined aquifers is described in detail in Gabrovšek and Dreybrodt (2001, 2004). The 1-D transport-dissolution model is reported in detail by Dreybrodt (1996). Therefore, we give only brief essentials here.

The simulation in time proceeds through a series of steady states because the time scale of fracture widening by dissolution is much larger than that of transient flow and transport. At each time-step, stationary solutions of flow, transport, and dissolution rates are used to calculate the change of fracture geometry within the time-step. We first calculate the hydrodynamics, based on mass conservation at the fracture intersections, the head loss relation for laminar flow along the fractures and the given boundary conditions. This yields a set of linear equations for the junction heads, which is solved by

preconditioned Conjugate Gradient method. To account for the free upper boundary of the unconfined aquifer, the calculation of heads is wrapped into an iterative procedure seeking that the head of junctions at the water table is equal to
135 their elevation above the base level (Gabrovšek and Dreybrodt, 2001;Gabrovsek et al., 2004).

We specify the calcium concentration $c_{in}$ and $p_{CO2}$ of the inflow solution at all input points. From these the equilibrium concentration, $c_{eq}$, with respect to calcite is calculated for closed system conditions with respect to $CO_2$. This way MC is included automatically. We calculate the dissolution rates in the fracture draining the input points by the rate law $F(c) = k_1\left(1 - c/c_{eq}\right)$ with $k_1 = 4 \times 10^{-11}$ mol cm$^{-2}$ s$^{-1}$ for $c < 0.9c_{eq}$ (Dreybrodt et al., 2005;Buhmann and Dreybrodt, 1985).

140 For $c > 0.9c_{eq}$ a nonlinear rate law $F(c) = k_4\left(1 - c/c_{eq}\right)^4$ with $k_4 = 4 \times 10^{-8}$ mol cm$^{-2}$ s$^{-1}$ is applied applied (Svensson and Dreybrodt, 1992;Eisenlohr et al., 1999). Next, we use the 1-D transport-dissolution model (Dreybrodt, 1996) to calculate the calcium concentration profile along all fractures, including the concentration of the solution leaving them. By following the order of decreasing heads, we select all nodes, where the concentrations of the inflowing solutions are known. We assume complete mixing of these solutions in the junctions before they enter into the conduits transporting the flow away. We
145 repeat this procedure until the input concentrations for all fractures are determined. From this, the new profiles of the fractures after a time step $\Delta t$ are obtained by applying the rate laws of dissolution. Then, the new flow rates are calculated and we repeat the entire procedure to obtain the temporal evolution of the net until some defined condition is met.

## 3. Mixing corrosion

In our Standard Scenario, we assume that the meteoric water after percolating through the vadose zone has become saturated
150 with respect to calcite when it reaches the water table. The upwelling water on its way from below also has reached saturation. Therefore widening of fractures by dissolution of limestone is possible only in the mixing zone by mixing corrosion (MC). For better understanding, mixing corrosion in the most general case is explained as follows.

Figure 3 depicts a plot of the Ca- equilibrium concentration in its relation to the $p_{CO2}$ in the solution. Whether a $H_2O$-$CO_2$-$CaCO_3$ solution is dissolving calcite can be judged from this equilibrium line. The equilibrium line (black) is given by
155 thermodynamics as (Dreybrodt, 1988) $c_{eq} = A(T)\,p_{CO_2}^{1/3}$ where $T$ is the temperature of the solution and $p_{CO_2}$ is the partial pressure of $CO_2$ in equilibrium with the solution. $A(T)$ is a constant depending on temperature only. A(T) = 11.3, 9.45, and 7.93 mmol L$^{-1}$(atm)$^{-1/3}$ at 10, 20, and 30°C respectively.

Hydrology and
Earth System
Sciences
Discussions

Open Access

EGU
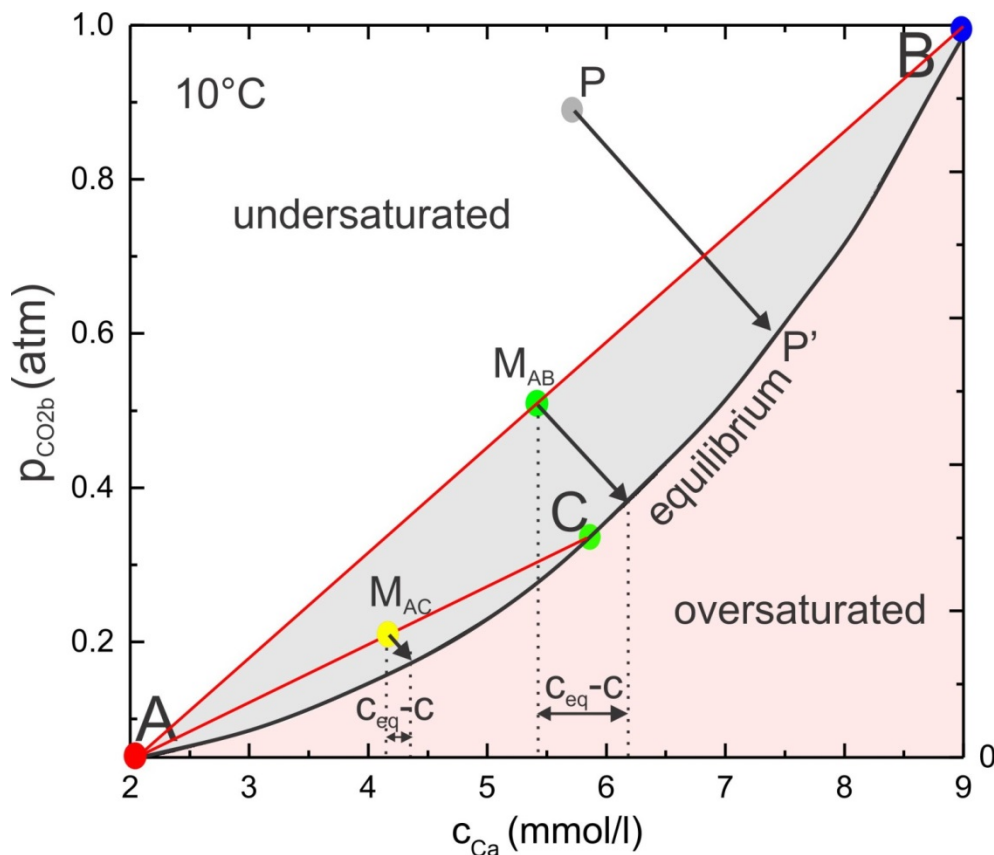
**Figure 3: Processes in mixing corrosion (MC), see text.**

The processes in MC are illustrated for $T = 10°C$, in Fig. 3. The chemical composition of each solution in a $H_2O$-$CO_2$-$CaCO_3$ system is defined by the ($c_{Ca}$, $p_{CO_2}$) coordinates. Each solution with chemical composition as given by point P above the equilibrium line (black) is undersaturated with respect to calcite whereas each point below the black equilibrium line is oversaturated and calcite can be precipitated from such a solution. Dissolution in fractures proceeds under closed system conditions where for each $CaCO_3$-unit dissolved one molecule of $CO_2$ is removed from the solution. The straight black arrows depict the reaction pathway under closed system conditions as used in all our scenarios. Equilibrium with respect to calcite is obtained, for example, when the line from P reaches point P'.

Classical MC, as a special case is defined when both, the mixing solutions A and B or C are saturated with respect to calcite. Due to the curvature of the equilibrium line, the mixed solutions $M_{AB}$ and $M_{AC}$ on the corresponding mixing lines (red) are undersaturated and can dissolve calcite. The amount of $CaCO_3$ dissolved can be read easily from the dotted arrow between the vertical dotted lines for the mixed solutions. To calculate $c_{eq}$, evolving from any point P, $M_{AB}$, or $M_{AC}$ one has to find the intersection of the reaction path lines with the equilibrium curve. This yields a cubic equation for $c_{eq}$.

## 4. Standard Scenario: Pure Mixing Corrosion

Figure 4 illustrates karstification of our Standard Scenario. The colour code depicts the rate of fracture widening in cm/Ky. Red is the maximal rate of 10 cm/ky, black is zero. The aperture widths of the fractures are shown by the bar code. The vadose zone is shown in light gray and the phreatic zone in black (no dissolution) or in colour (dissolution active).

Dissolution is active by mixing corrosion in the fringe where meteoric water and water from below mix (see also Figs. 2 and 3). At the beginning (Fig. 4a), a fringe of moderate dissolution rates increases the hydraulic conductivity in this region.

After 500 years (Fig. 4b) high dissolution rates are seen (orange) close to the input region of hypogene water. Below that region of enhanced dissolution, one finds black widened fractures where dissolution has stopped. Evidently, the mixing zone due to the change of hydraulic properties has moved upwards. In the middle section, the region of mixing has become wider. Close to the exit of water dissolution is restricted to a narrow band with high dissolution rates.

After 5000 years (Fig. 4c) the region of dissolution has moved further upwards leaving a region of widened fractures below (black). A main channel has formed to which dissolution is restricted. It widens uniformly and stays stable as can be seen at 30000 years of evolution (Fig. 4d).

This is also illustrated in Fig. 5 that shows rates of fracture widening (green) in cm/year and the aperture widths (red) of the horizontal fractures along the vertical transects $p_1$, $p_2$, and $p_3$ as depicted in Fig. 4a. Although there is some variation in the fracture widening its region is restricted to a depth of 100 to 113 m where the rates stay almost constant in time with maximum rates of about several cm/ky. Therefore, the aperture widths increase linearly in time to a width of about 50 cm after 30000 years.

Hydrology and
Earth System
Sciences

Open Access

EGU

Discussions
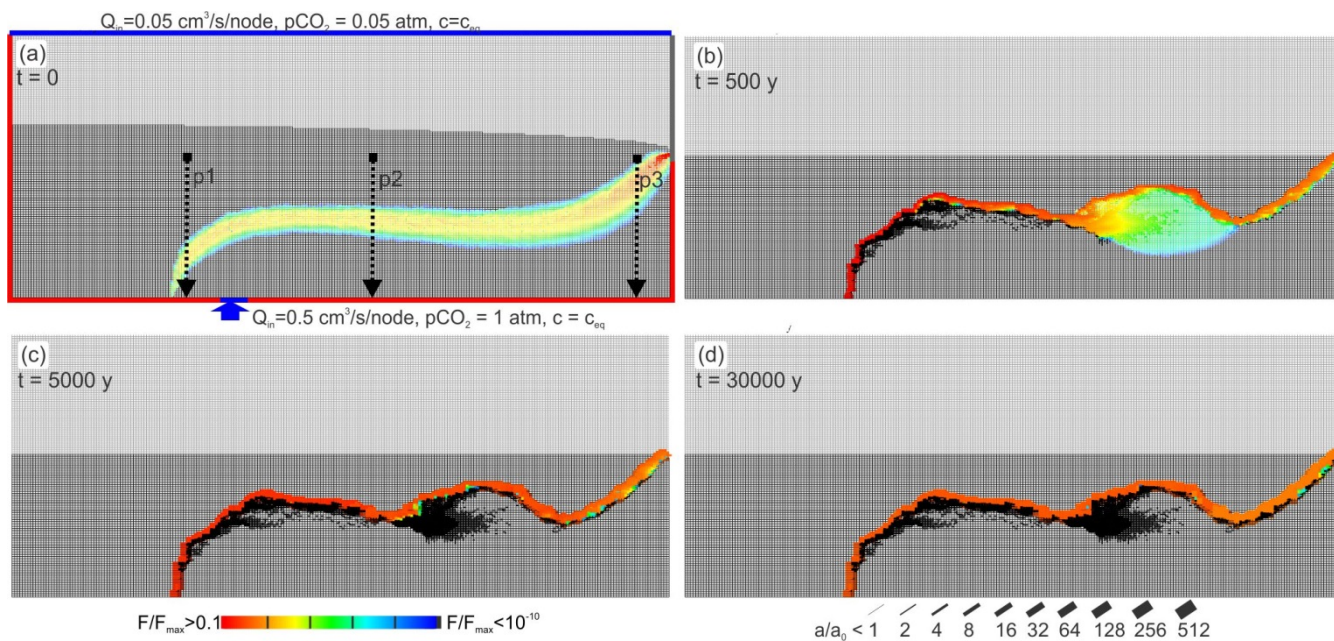
**Figure 4: Temporal evolution of the Standard Scenario with MC exclusively. The colour code depicts rate, F, of fracture widening divided by the maximal widening $F_{max}$ = 10 cm/ky in the net. Aperture widths, a, of fractures are shown by a bar code in units of $a_0$, the initial average aperture width. After 5000 years the pattern is stable in time and all fractures widen with rates almost constant in time. $P_1$, $P_2$, $P_3$ are the positions of the transects of fracture aperture widths and rates of fracture widening shown in Fig. 5.**
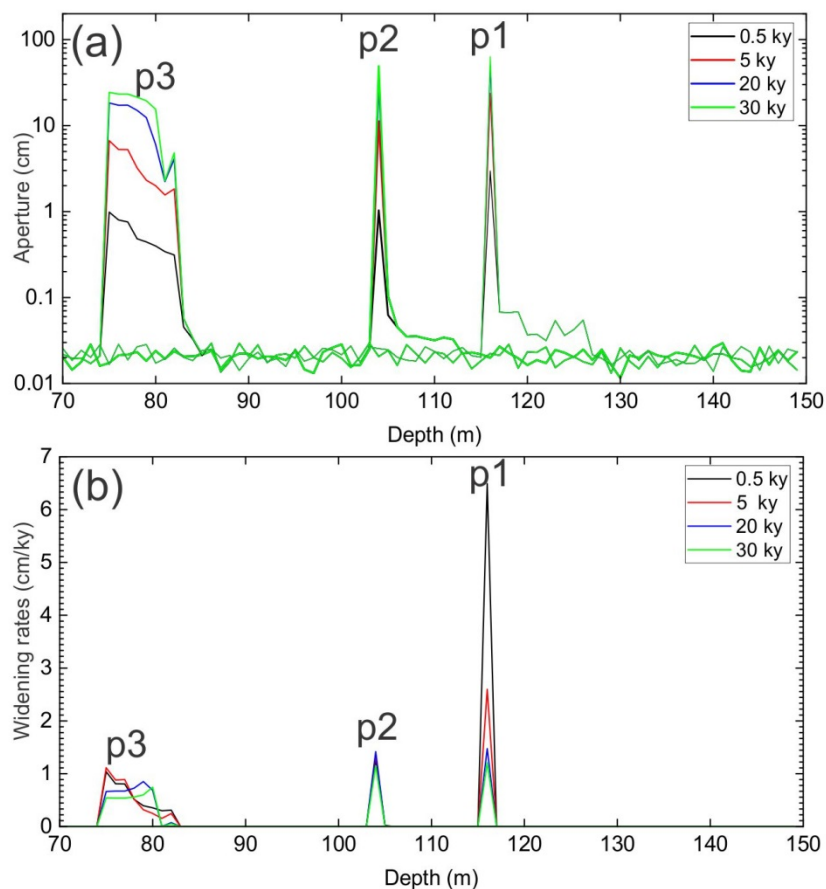
**Figure 5: Transects of aperture widths and rates of widening of the horizontal fractures along the positions $p_1$, $p_2$, and $p_3$ in Fig. 4a**.

205

To explore the influence of the $p_{CO2}$ in the upwelling water we have performed a simulation with $p_{CO2}$ = 0.2 atm and everything else as in the Standard (not shown). The result is very similar to the Standard. But due to the smaller $(c-c_{eq})$ = 0.1 mmol/l at 0.2 atm (see Fig. 3) dissolution rates are reduced by almost one order of magnitude compared to 0.8 mmol/l at 1 atm (see Fig. 3). Consequently, the evolution to similar conduit (fracture) dimensions is delayed accordingly.

210

**5. Influence of the ratio q/Q**

As already stated, the position of the mixing fringe depends on the input ratio $q/Q$. Therefore, we have studied the evolution with three different recharge rates of rain water corresponding to 400, 800, and 1600 mm/year and constant input of hypogene water from below. Figs. 6a, b, and c exhibit the distribution of dissolution rates and fracture aperture widths after 215 44000 years. In all cases, one finds a fringe of karstification that is related to the location of the mixing zone. With

11

increasing recharge by meteoric water this fringe is shifted downwards. Figure 7 depicts the profiles of the aperture width of the horizontal fractures close to the input of hypogene water and close to the output at the spring. The profiles of aperture widths are very similar for all three cases, because the mixing of the waters does not depend on the position of the mixing zone.
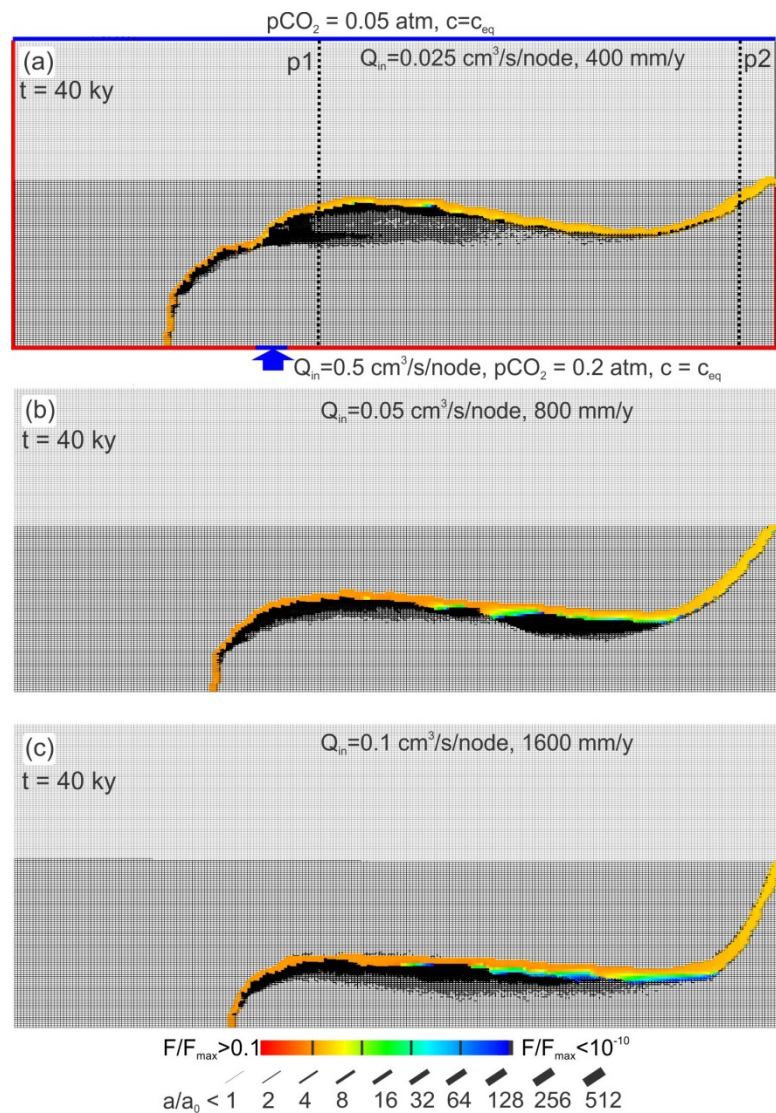


220

**Figure 6: Cave pattern after 40000 years for various recharge rates Q, a) 400 mm/year, b) 800 mm/year, c) 1600 mm/yea and constant recharge from below. With increasing recharge, the flow domain of meteoric water increases and the fringe of mixing is shifted downwards. To show that even low $p_{CO2}$ in the upwelling water creates substantial karstification we have used $p_{CO2} = 0.2$ atm. Everything else as in Standard Scenario.**

225

Hydrology and
Earth System
Sciences
Discussions

Open Access

EGU
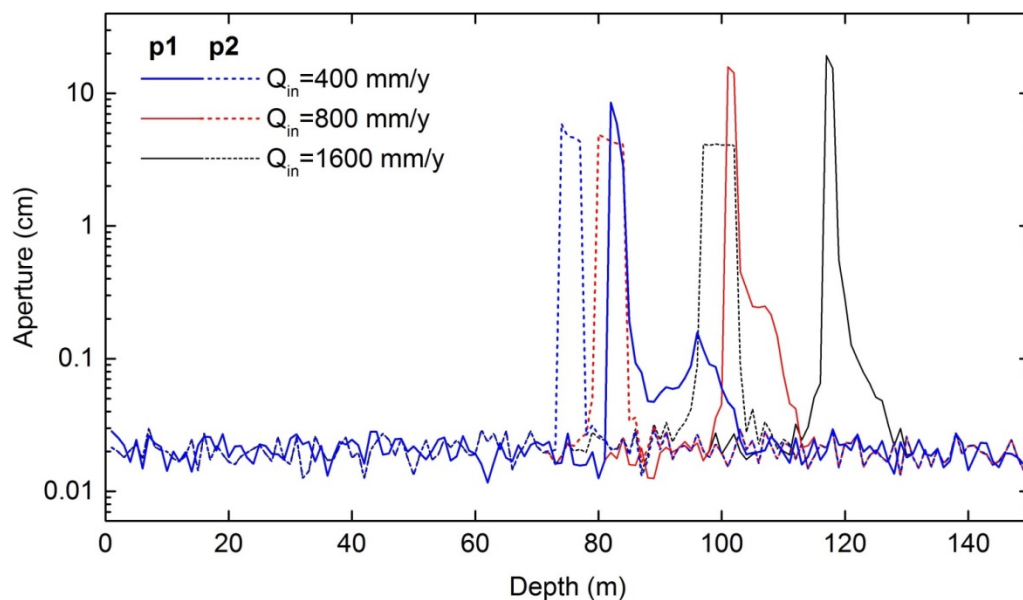
**Figure 7: Vertical profiles of horizontal fracture aperture widths along the positions p1 and p2 shown in Fig. 6. after 40 ky of evolution.**

## 6. Standard Scenario. Meteoric recharge changes in time

230    In all cases treated so far we have assumed that meteoric recharge is constant in time. This assumption is not realistic. In nature, meteoric recharge does fluctuate and consequently the location of the mixing fringe will change its position accordingly. Therefore karstification may not be longer limited to the initial narrow fringe but could also be active between the fringe positions of maximal, $Q_{max}$, and minimal, $Q_{min}$, meteoric recharge.

To reveal the evolution under such conditions we studied the following scenarios. In the first, meteoric recharge is low at
235    400mm/year during the first 10,000 years of evolution. Then recharge is switched to a high value of 1,600 mm/year. In the second scenario we start with the high recharge and switch to the low one after 10,000 years. The results are shown in Fig. 8. The panels on the left hand side illustrate the temporal evolution when the initial input is low. In the beginning, the mixing zone is close to the water table due to the small input of rainwater. Dissolution and correspondingly widening of the fractures is restricted to this region, which gains higher hydraulic conductivity than its neighboring regions. This focuses flow of both,
240    the flow domain from the input below and the flow domain of the rain water into the region of increased hydraulic conductivity during the first 500 years. A channel develops reaching the dropping water table and then after looping down approaches the spring. This channel attracts all flow and even when the model switches to higher input of rainwater after 10,000 years the further evolution proceeds along this channel as depicted in the lowest panel after 15,000 years.

The right hand side panels show the temporal evolution when the initial input of meteoric water is high at 1600 mm/year and
245    then after 10,000 years switches to the low value of 400 mm/year. Due to the high input the mixing zone is forced deeper

Hydrology and
Earth System
Sciences
Discussions
EGU
Open Access

into the aquifer. In analogy to the left hand side scenario in this region high conductivity is created that further determines the evolution of a channel

deeper in the aquifer that does not change its position even when the input of rain later is reduced drastically after 10,000 years.

250 In summary: The evolution of caves is highly determined by its initial phase of evolution and restricted to the regions where widening of fractures occurs initially. This is due to a positive feedback loop that exists initially. Widening of fractures attracts flow increasing dissolution rates that cause widening of fractures and so on. However, this feedback exists only in the beginning when the rates are low and breaks down later when the dissolution rates remain finite.
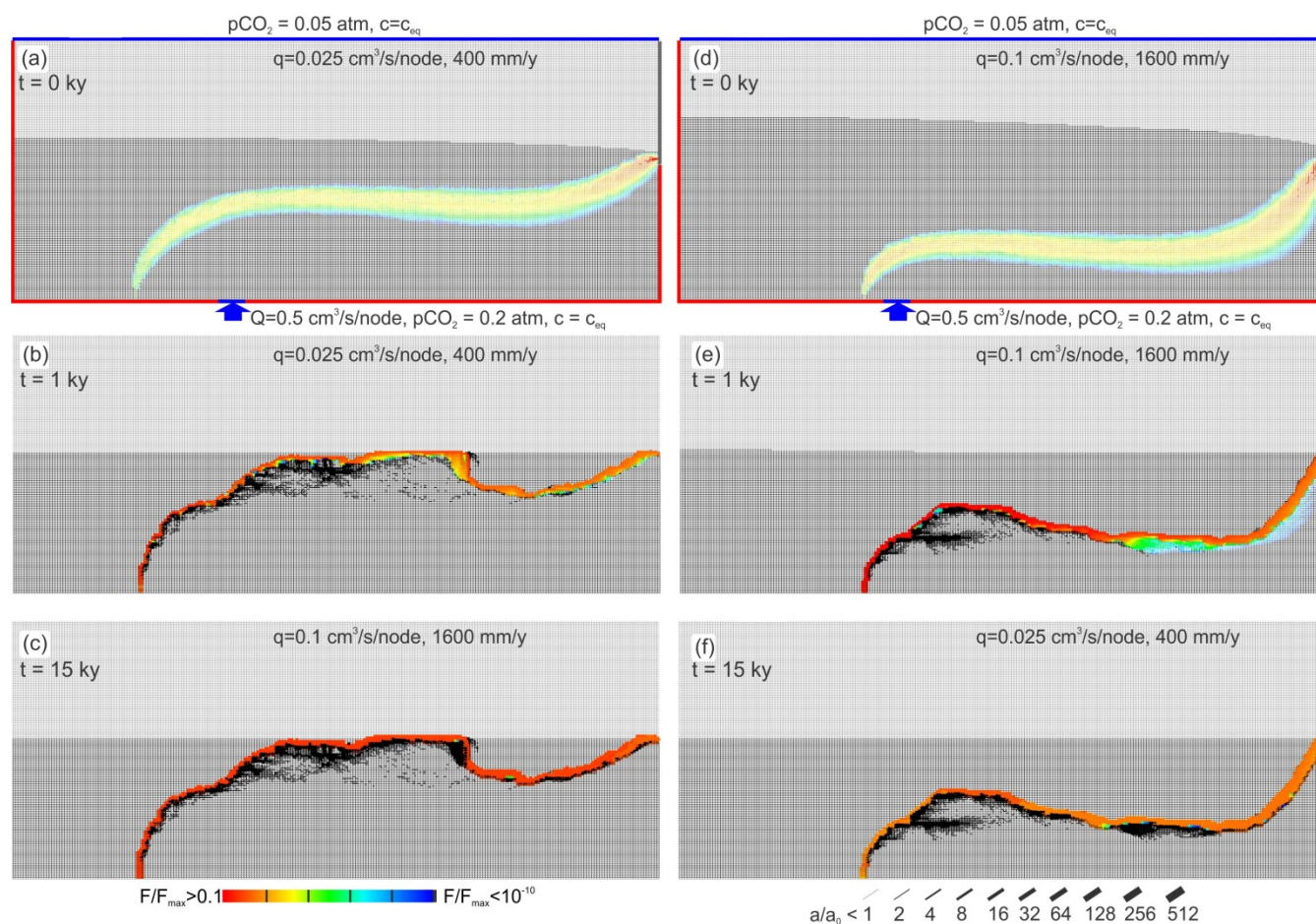


255 **Figure 8. Temporal evolutions when meteoric recharge changes in time. Left hand side panels: Initial input is 400 mm/year and stays constant for 10000 years, and then it switches to 1600 mm/year constant in time. Right hand side panels: Initial input is 1600 mm/year and stays constant for 10000 years, and then it switches to 400 mm/year constant in time.**

Hydrology and
Earth System
Sciences
Discussions
Open Access
EGU

260    To illustrate this mechanism we have explored the following scenario. We have inserted a region where all fractures have
initial apertures of $a_0 = 0.04$ cm as indicated in Fig. 9a. Fig. 9b depicts the evolution after 1200 years. The right hand side
column shows the evolution of the corresponding scenario without the widened region (Standard Scenario, Fig. 4). It is
clearly seen that the zone of widened fractures attracts flow. The mixing zone is pushed upwards and the conduits of the cave
system are located in this zone of wide fractures. It should be stressed at that point that regions with doubling of the initial

265    aperture widths are sufficient to change the patterns of the cave systems drastically. Average initial widening of aperture
widths is about $10^{-4}$ cm/year in all scenarios discussed  in this work. Accordingly, only the very early state (200 years) of
cave evolution is sufficient to create regions of doubled aperture widths that determine the future evolution of the cave
system.
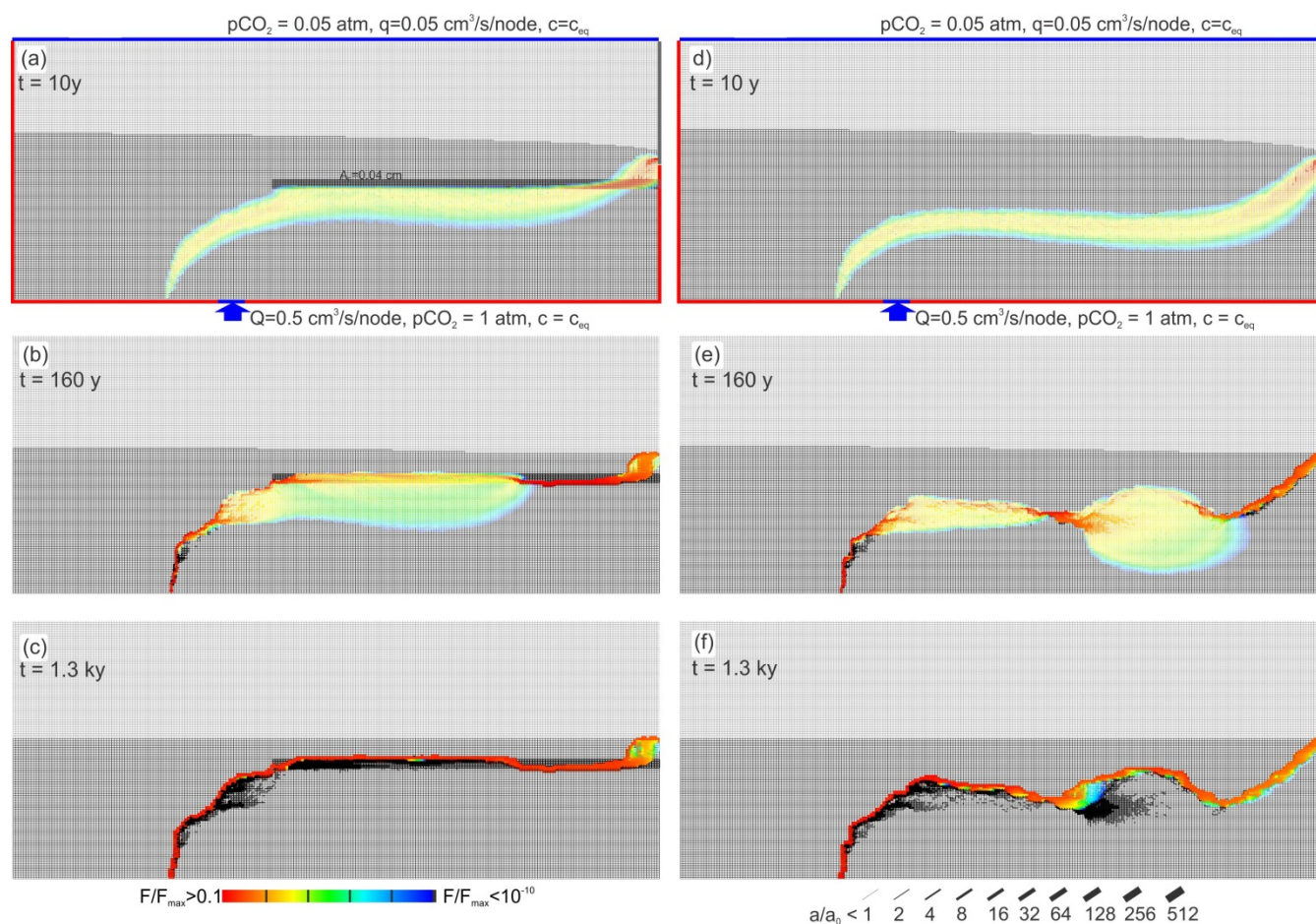


270

**Figure 9: Evolution of the Standard Scenario with region fractures with larger initial aperture ($a_0 = 0.04$ by black region, a-c) compared to the evolution of the Standard Scenario on the right hand side (d-f). The region of enlarged fractures dominates the evolution.**

## 7. Standard Scenario with input of aggressive water

275 So far we have assumed that the upwelling water is saturated with respect to calcite. If, however, the deep water on its way upwards does not pass any limestone formation it will be undersaturated with respect to calcite. In the extreme case, its calcium concentration is zero. We have modeled this extreme case for the conditions $q = 0.05$ cm-3/node corresponding to 800 mm/year, $Q = 5$ cm3/node $c_{in}/c_{eq} = 1$ and $p_{CO2} = 0.05$ atm at top $c_{in}/c_{eq} = 0$ and $p_{CO2} = 1$ atm. at the bottom. The temporal evolution is shown in Fig. 10.

280
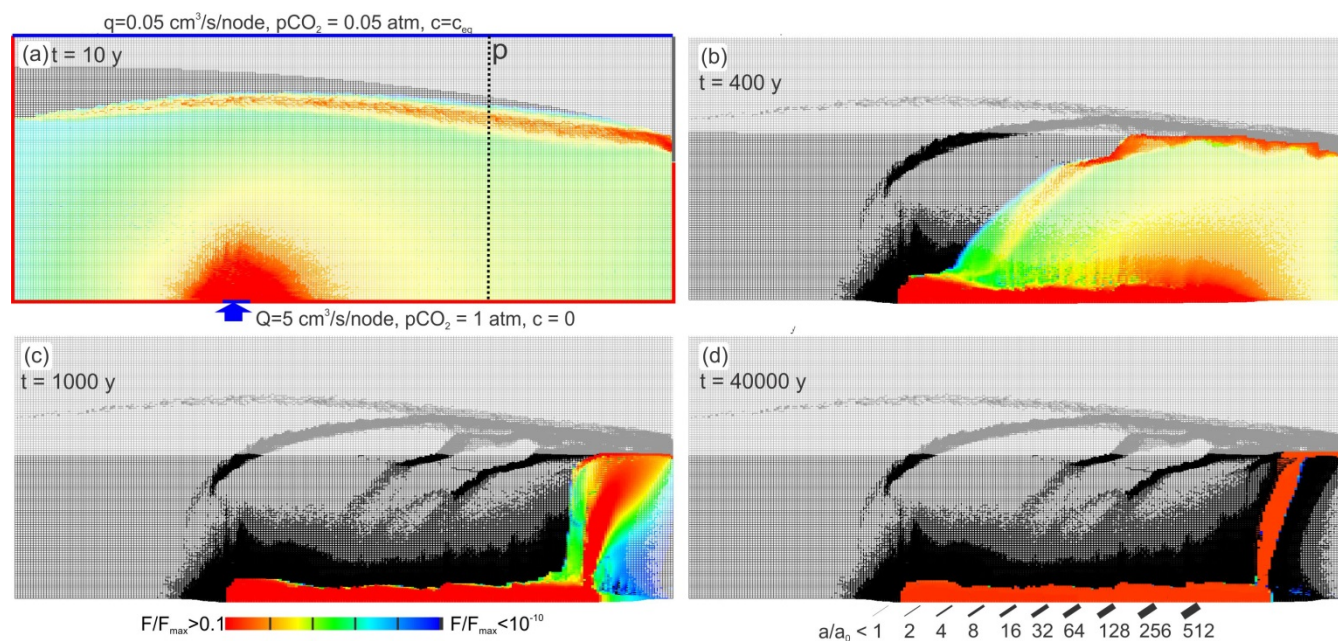


**Figure 10: Standard Scenario with upwelling water undersaturated with respect to calcite, cin = 0, and input raised to 5 cm3/s. The red region indicates high rates of fracture widening.**

285 The flow domain of the water from below extends close to the water table. There MC is active as indicated by red fringe. Due to the high hydraulic conductivity created by the aggressive water from below the water divide drops to the highly conductive region where further dissolution remains active.
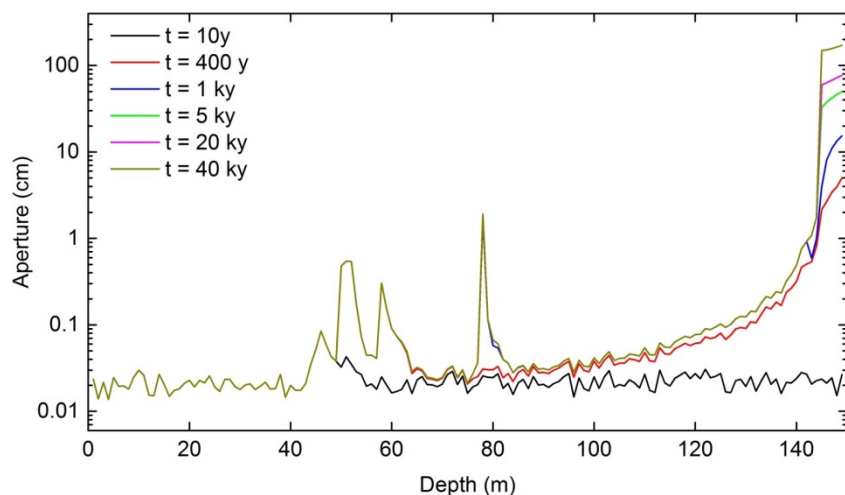
**Figure 11: Aperture widths of horizontal fractures along a vertical profile at position marked by dashed line (p) in**
**Fig. 10a. Note that in the late evolution widening of fractures is restricted to the fractures at base level.**

In the initial state (Fig. 10a) two regions of dissolution are seen. The upwelling water is highly aggressive and creates a
region (red) of high dissolution rates in the input region. More distant from the input this water approaches saturation as one
can see from the change of colour from red to blue. Due to the high input rate of the upwelling water, the water table is
initially higher than in the standard scenario.

At the water divide between the flow domains the upwelling water is mixed with the meteoric water from the surface and
gains renewed aggressivity by MC as can be seen from the red fringe in the mixing zone. The mixing zone is initially above
the base level. Due to increasing hydraulic conductivity the mixing zone drops as karstification proceeds, leaving behind the
widened inactive regions in the vadose and phreatic zone (Fig. 10b). After 1000 years (Fig. 10c) the region of dissolution
has dropped to the base level. The mixing zone is limited to the outflow region. Dissolution is active only in the region at
the bottom of the aquifer where inflowing water from below is guided due to the high conductivity that has been created
there. At the end of its horizontal part the water rises still maintaining its dissolution power. The flow domain of the water
from below is restricted to the region of highly widened fractures. In the black region of the aquifer dissolution has stopped
leaving a complex pattern of widened fractures. This structure of the aquifer is stable in time as can be seen from the panel at
40000 years (Fig. 10d). In the red region fractures widen continuously creating complex caves. The aperture widths of the
horizontal fractures along vertical transects as indicated in Fig. 10 a are shown in Fig.11.

Hydrology and
Earth System
Sciences
Discussions
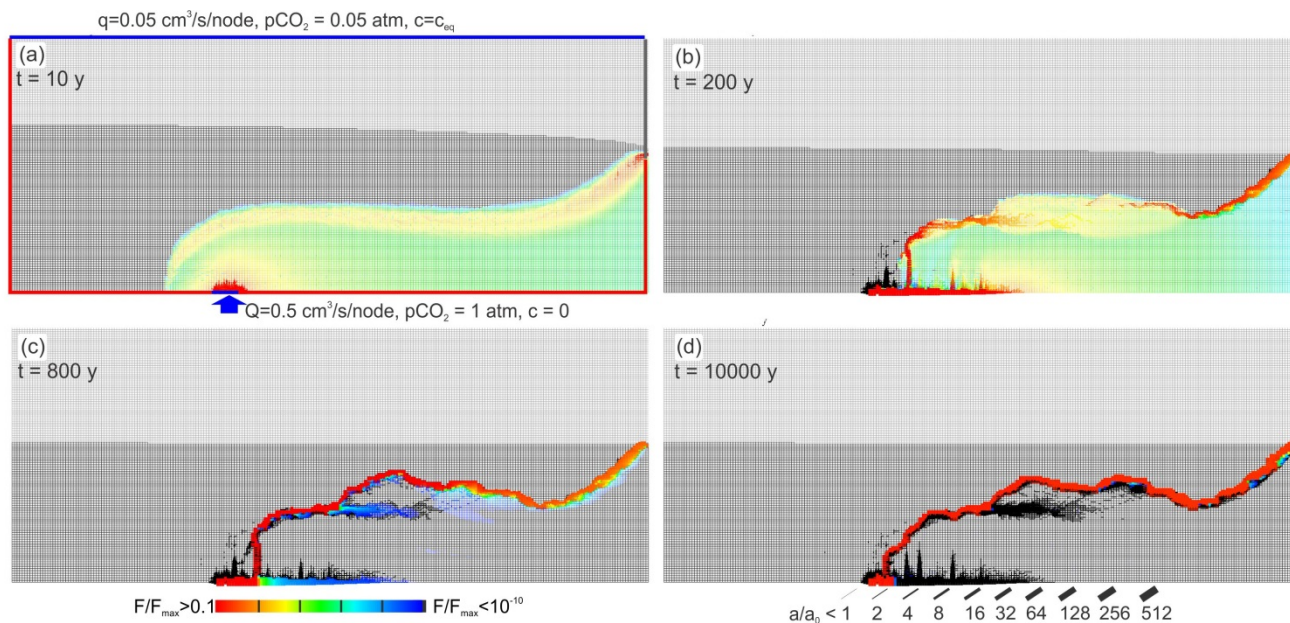


**Figure 12: Standard Scenario, but upwelling water is undersaturated with respect to calcite, $c_{in}$ = 0. The red region**
310 **indicates high rates of fracture widening. The highly aggressive water is channeled to the mixing zone at the water**
**divide.**

In order to find the influence of flow rate, Q, of the upwelling water we have reduced Q from 5 cm- 3/(node and s) to 0.05
cm/(node and s) and have left everything else as in Fig. 10. The result is shown in Fig. 12. Because of the reduced input, Q,
315 the region of high dissolution rates (red) is much smaller and the mixing zone at a lower position compared to Fig. 10. After
200 years (Fig. 12b) dissolution is active in both, the plume of upwelling water and in the mixing zone. At 800 years (Fig.
12c) flow is mainly along the channel that has evolved along the mixing zone and only there do the fractures widen. This
pattern remains stable as can be visualized after 10,000 years (Fig. 12d)

To complete our understanding of dissolution patterns we have addressed the question: what happens when both, the
320 meteoric surface water and the upwelling water from below are undersaturated with respect to calcite. To study this
systematically we compare the results of three scenarios:

**Scenario A)** The meteoric water that enters the water table is undersaturated with concentration $c_A = 0.9 c_{eq}^A$ , $p_{CO2}$ = 0.05
atm and $q$ = 0.05 cm³/(node s). The water from below is undersaturated as well with $c_B = 0.9 c_{eq}^B$ , $p_{CO2}$ = 1 atm and $q$ = 0.5
cm³/(node s).

325 **Scenario B)** The meteoric water is undersatured $c_A = 0.9 c_{eq}^A$ and the upwelling water is saturated, $c_B = c_{eq}^B$

**Scenario C)** Both, the surface water and the upwelling water are saturated with respect to calcite. This case is already
illustrated in Fig. 4, right hand side panels and discussed there.

All other conditions in Scenario A and Scenario B are equal as in Fig. 4.

330 The temporal evolution of scenario A is illustrated in Fig. 13. In the beginning (panel a) we observe three regions of dissolution, the first at the water table where the aggressive surface water enters (yellow fringe). In the zone where rainwater mixes with the water from below renewed aggressivity arises by MC (yellow region). Finally, a plume extends from the input region of aggressive water from below (yellow). After 120 years (panel b) enhanced dissolution is observed in the bottom region where water from below enters and in the fringe of mixing (red). After 1300 years (panel c) dissolution at the

335 bottom is restricted to the input nodes. Mixing with high dissolution rates becomes restricted to a narrow band. Below this an extended zone of reduced rates (blue) is seen. Dissolution at the water table is similar to that of past times before. This pattern remains stable (panel d,e) until 30,000 years and thereafter. Most of the flow is focused to the water table cave and the cave system below. The black regions below show fractures with increased aperture widths invaded by saturated solutions. Therefore, dissolution in this region is absent.
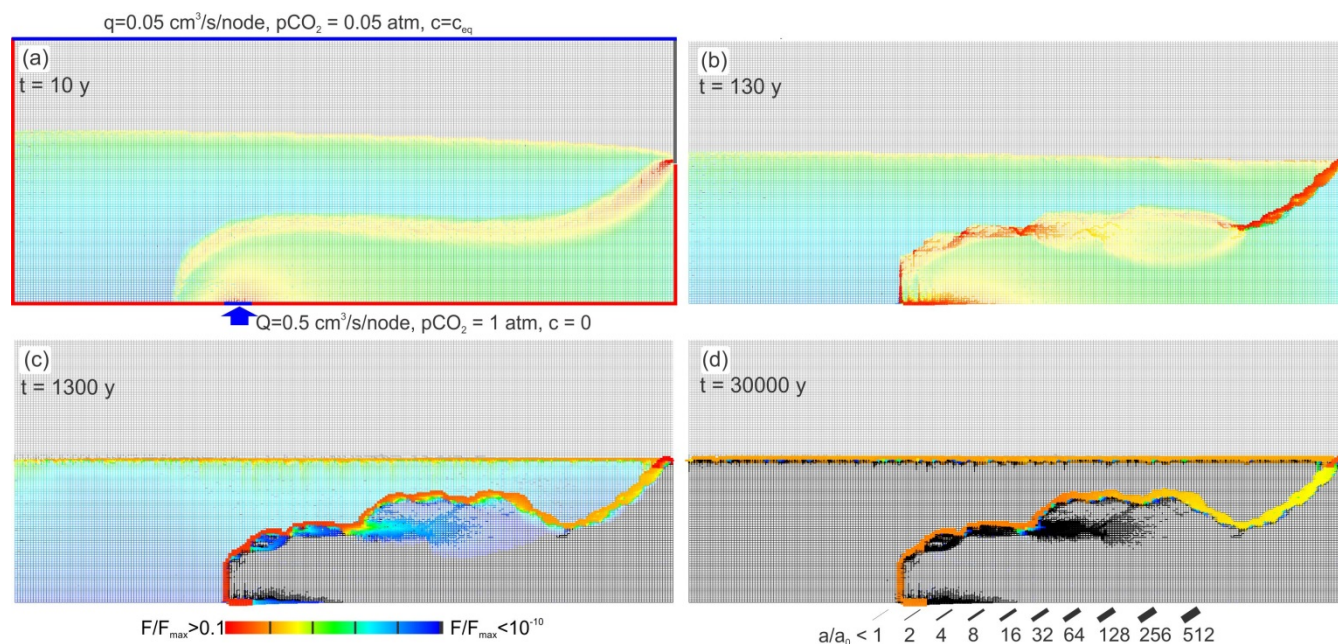


**Figure 13: Temporal evolution of scenario A. See text.**

Figure 14 shows evolution of Scenario B (saturated upwelling water, undersaturated meteoric input). In the beginning, two regions of dissolution are seen. The undersaturated rain water establishes a region of fracture widening at the water table.

345 Mixing of rainwater that has become almost saturated on its way down with the upwelling water creates a fringe of mixing corrosion. There a cave system is evolving. At the same time, the meteoric water widens the fractures at the water table creating a zone of high hydraulic conductivity, which in time drains most of the meteoric water to the output on the right. Therefore, the meteoric water does no longer intrude downwards and the mixing corrosion is no longer active. The entire

region below is invaded by the upwelling water that is saturated with respect to calcite ( black region) and further dissolution

350    there stops. The water table cave however continues to grow.
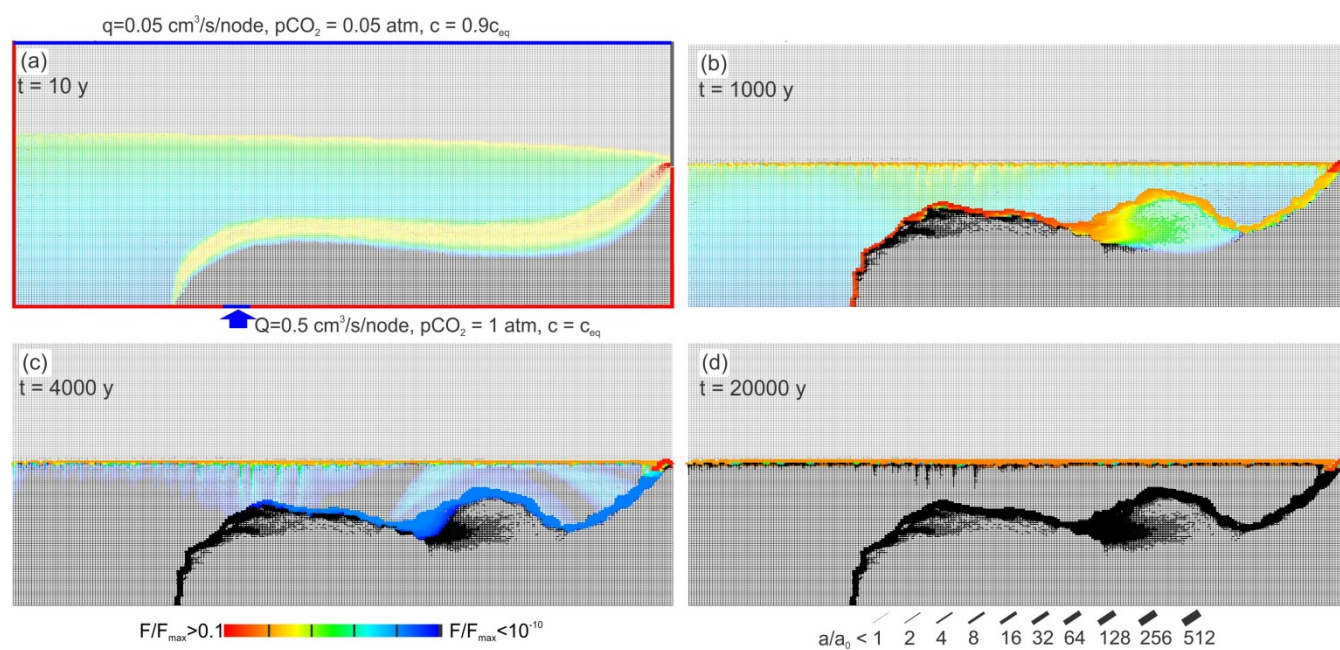


**Figure 14: Temporal evolution of scenario B. See text**
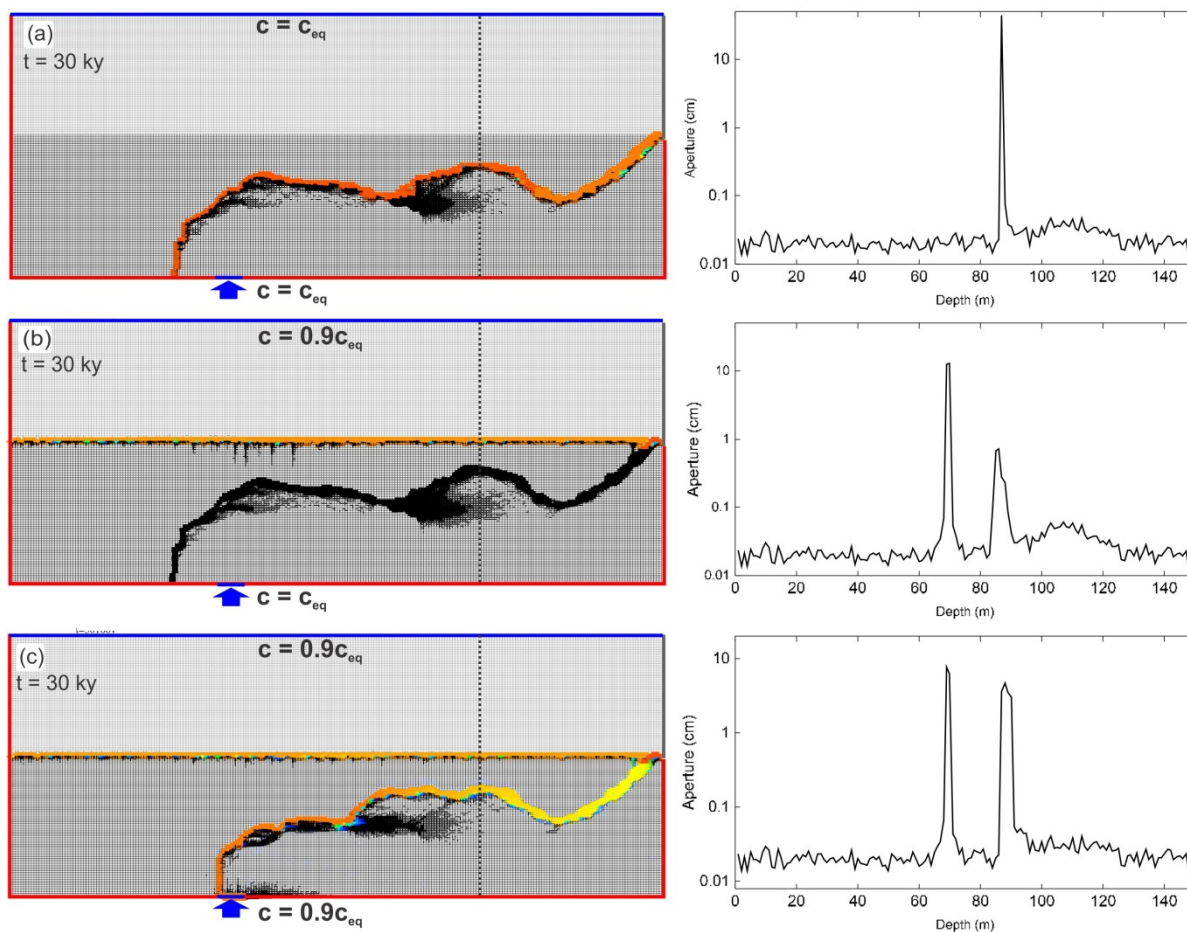
**Figure 15: Final evolution states of scenario A, Fig.13, scenario B, Fig. 14, and in Standard Scenario C, Fig. 4. Panels on the right show widths of horizontal fractures along profile lines shown in figures a-c.**

Figures 15 a,b,c illustrates the three final evolution states of scenarios A, B and C, presented in Fig.13. 14, and 4. Panel a depicts the situation when both waters are undersaturated. Here due to the aggressive water from below dissolution rates along the mixture fringe are enhanced and flow from below occupies this region and that below it. Panel b depicts the final state when the meteoric water is aggressive only, as in Fig. 11. By the increasing hydraulic conductivity at the water table most of the flow of meteoric water is directed along this region. Mixing with the water from below is also restricted to this region where the water creates high dissolution rates.

365 In panel a, both, the meteoric water and the water from below are saturated with respect to calcite as in Fig. 4. Dissolution results from MC and lasts during the entire time of evolution. The right hand side panels 14 d, e, f illustrate the aperture widths of the horizontal fractures along the vertical transect as indicated in the corresponding left hand side.

## .8. Mixing Corrosion-fringe-instability in the mixing zone.

In all scenarios with pure MC discussed in this work we observe a common behavior during the early time of cave evolution.
370 This is shown in Fig. 16. The left-hand side panels repeat the evolution already shown for the Standard Scenario in Fig. 4. At the beginning when dissolution has not yet been active, a wide fringe of mixed waters extends to both sides of the water divide between the two flow domains. At the output where flow is constricted to a narrow region the fringe of mixing is also narrow and one to one mixing occurs in its middle creating maximal widening of fractures as can be read from the red fractures. Therefore, flow is focused and the cave develops in this narrow region propagating upstream. This is a common
375 feature in all scenarios where dissolution in a mixing fringe is of relevance.

After a short time the shape of the fringe is distorted (Fig. 16c). It is constricted to a narrow zone. In the middle of it dissolution rates are high as seen by red fractures. Beyond this constriction, an extended region of mixing with low rates of widening extends until it is squeezed again because its flow is channeled into the cave that propagates upstream.

The first constriction arises by an instability caused by chance due to the heterogeneity of the fracture aperture widths.
380 Somewhere in the mixing zone, dissolution rates are maximal compared to the neighboring ones (Fig. 16b). They create a narrow region that attracts flow increasing further favorable mixing. This causes a feedback loop as already described. At the end of this region, flow is dispersed and the extended zone of mixing is created.

To show that it is the heterogeneity of the fracture widths that causes the instability we have investigated what happens (not shown here) when all fracture have equal uniform aperture widths of 0.02 cm. Here during the time ranges explored in Fig.
385 15 no instability occurred. This gives a warning in the reliability of digital models that are high idealizations of nature.

To give further support to our interpretation in the right hand side panels (Fig 16 d-f) we show the evolution of a scenario where a zone of wider fractures (0.04 cm) has been introduced as indicated by the black rectangle. In this case the constriction occurs exactly in this region.

Hydrology and
Earth System
Sciences
Open Access
Discussions
EGU
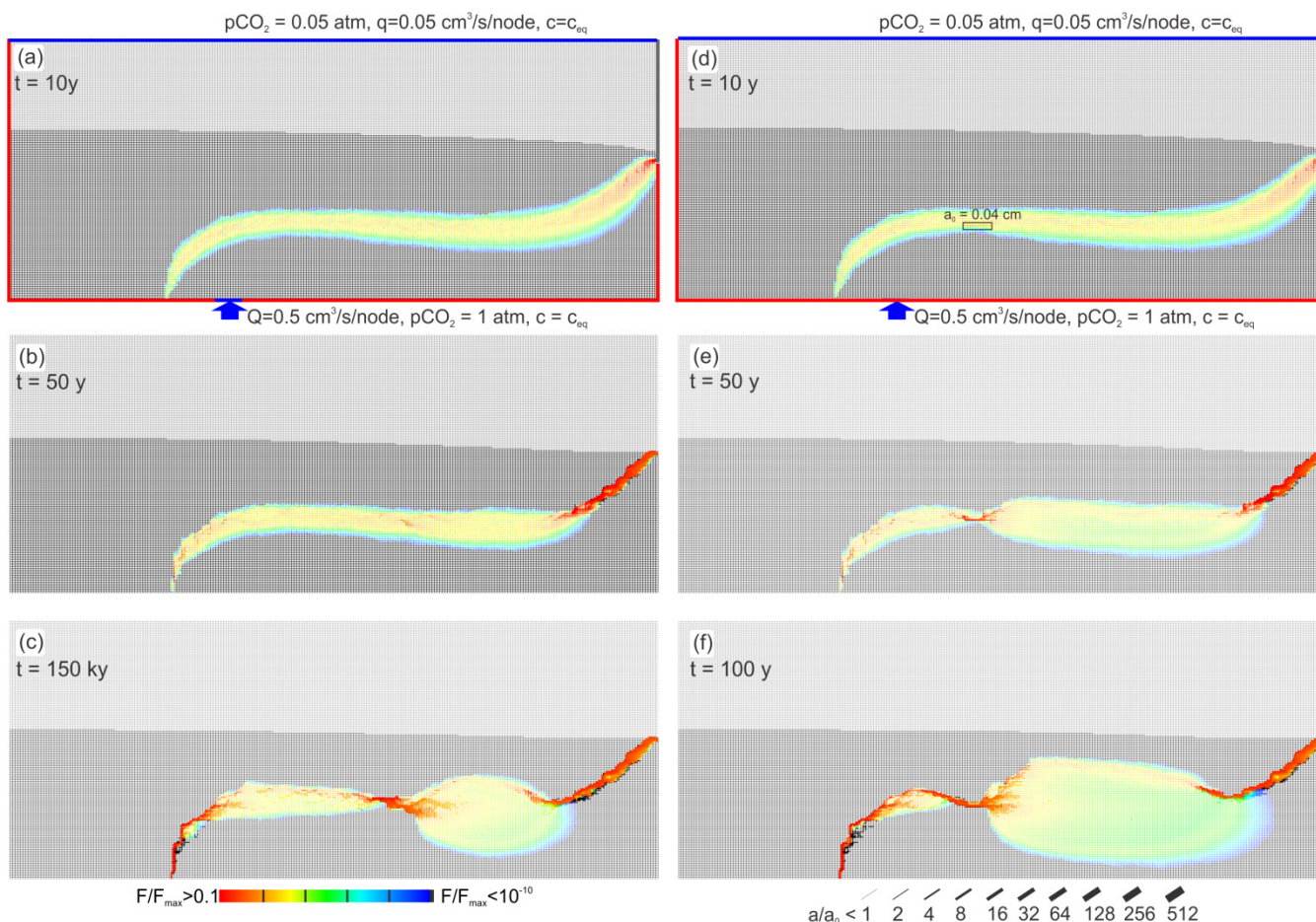
390

**Figure 16: Evolution of mixing zone instability and constriction. a,b,c: Standard case (see Fig. 4); d, e, f: Standard case, where instability was triggered by assigning initial aperture a0 = 0.04 cm to set of 4 horizontal fractures, marked by rectangle in panel d.**

395 One would expect that such constrictions should occur again in the downstream region. This, however, is prevented by focusing into the narrow output region. Therefore, we have extended the modelling domain from 500 m to 1400 m in the horizontal direction. The result is shown in Fig. 17. In the beginning, the fringe of mixing extends along the entire length of the domain. However, in the further evolution a series of constrictions arise as expected.
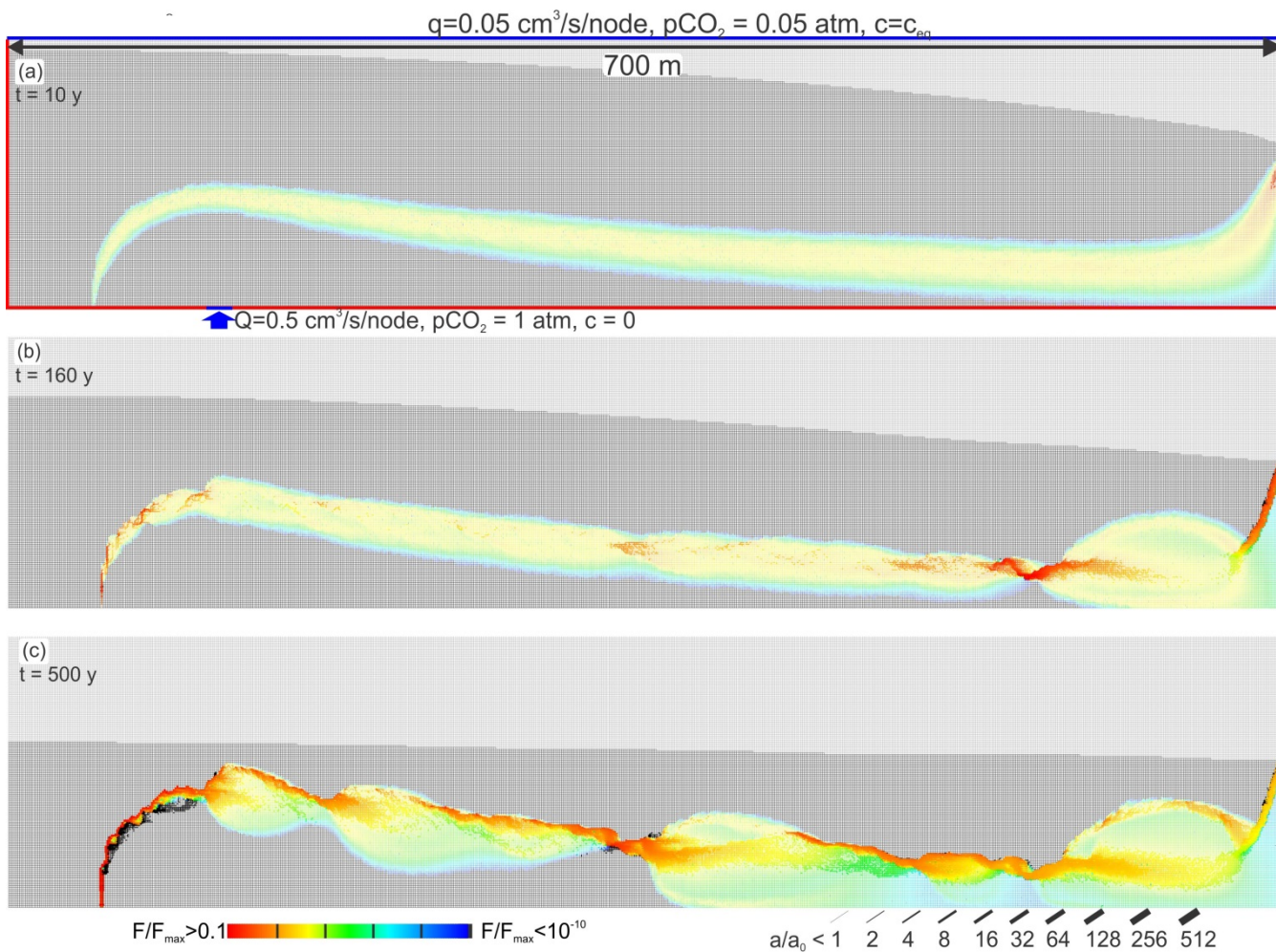
**Figure 17: Standard scenario with horizontal extension of modelling domain from 500 m to 1400 m. Several constrictions occur downstream**

## 9. Impact of boundary conditions

In all our scenarios so far outflow was focused to the seepage face. To explore the impact of boundary conditions to the

405    evolution of karst by MC we have replaced the non-flow boundary below the seepage face by a constant head boundary with

head zero. In nature, this could be a river or a lake located at the rim of the rock massif that hosts the cave system.
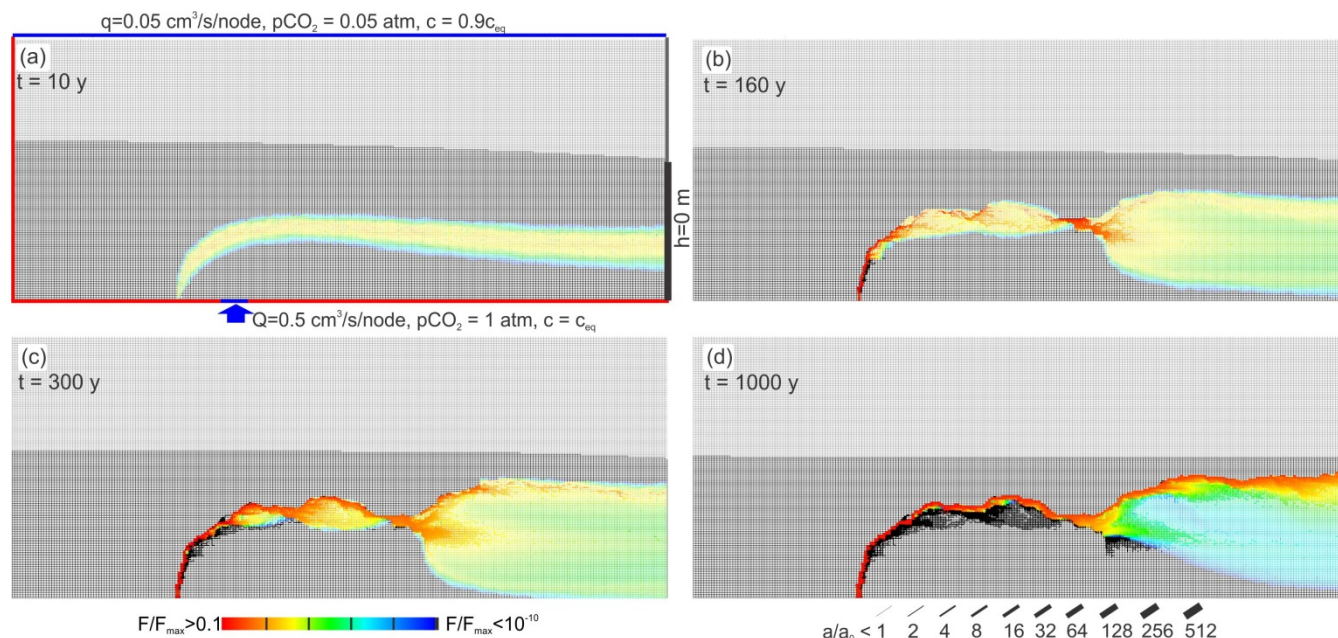


**Figure 18:   Change of boundary conditions on the outflow to constant head conditions.**

410    The result is illustrated in Fig. 18.  As in all scenarios that we have reported, a mixing fringe is present in the beginning. It

shows two constrictions downstream due to the MC-instability. From there a wide mixing zone extends with large widening

of fractures at its upper rim. These regions of high dissolution rates determine the location of the cave. This shows that the

MC-fringe-instability is a unique property of the MC-fringe independent of the specific output boundary conditions.

## 10. Pattern of flow

415    To further illustrate the origin of the mixing zone instability we have investigated the flow pattern and its relation to

dispersive mixing. Figure 19 presents the Standard Scenario with arrows presenting average direction and flow rate in 5x5

sub domains. Length of the arrow presents the flow rate in a sub domain normalized to the flow rate in the sub domain with

maximal flow. This way flow lines can be envisaged easily.

Panel a) depicts the pattern of flow rates at the onset of dissolution. In the upper flow domain resulting from meteoric input

420    all arrows point downwards and all flow lines that can be envisaged from these arrows are first directed downwards, then

they bend and become almost parallel to the upper fringe of the mixing zone until they are directed to the outflow. There the flow lines are squeezed into a narrow band and accordingly their amount increases as can be seen by the long arrows. The flow lines inside the mixing zone and those touching it at its rims are almost parallel to each other. The flow lines in the lower flow domain originating from the hypogene input rise from the input region then bend and become parallel to the

425    lower fringe of the mixing zone. Finally, they are directed towards the output.

Mixing between the surface water and the hypogene water is possible only where the flow rate vectors are located in the mixing zone or close to the water divide. One by one mixing and accordingly, widening of fractures is enhanced in all regions in the mixing zone where the flow vectors have vertical components. These regions are indicated by shaded rectangles in panels a,b, c and d). From these one understands why dissolution rates are high at the output and at the region.

430
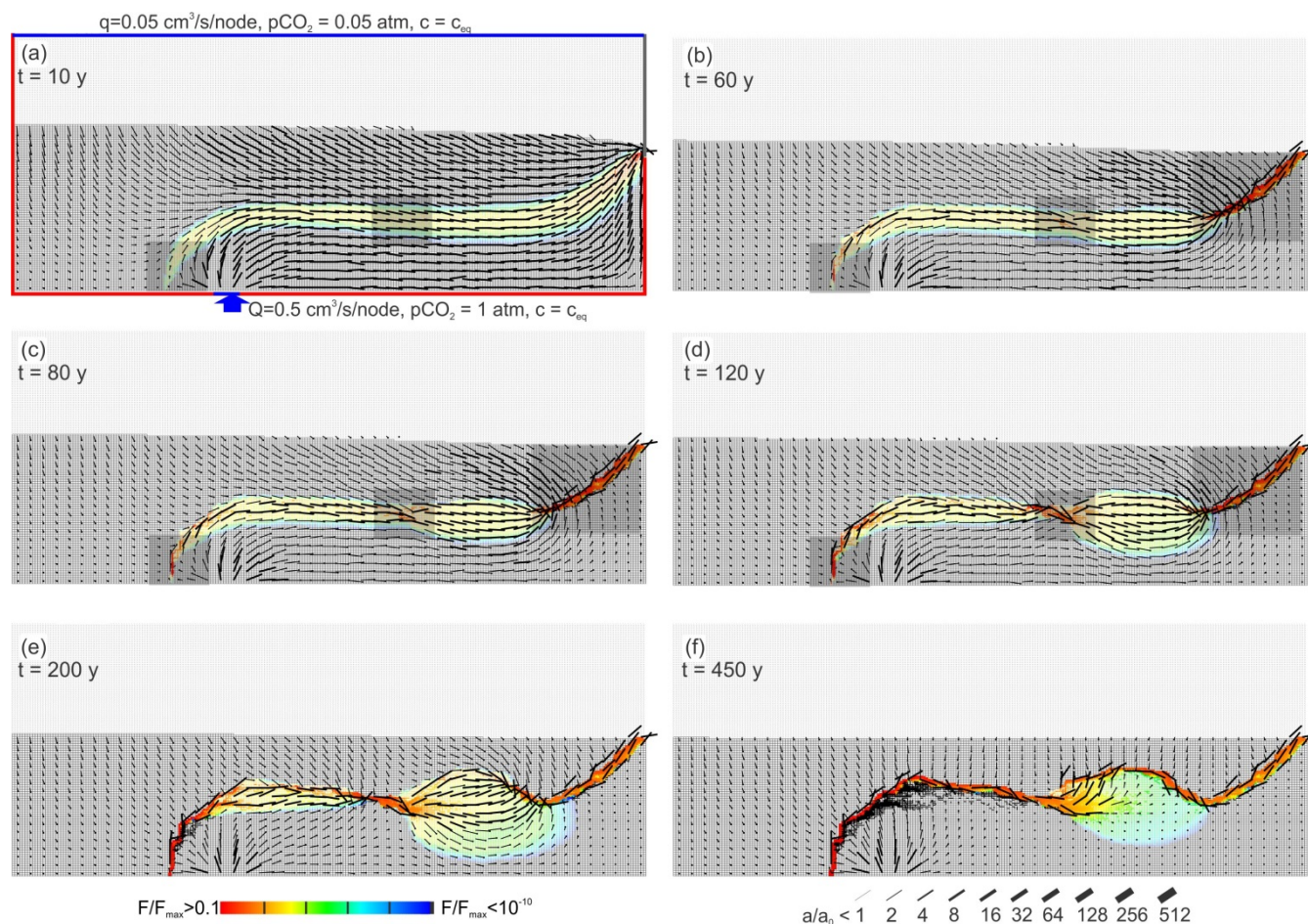


**Figure 19: Patterns of flow lines for the Standard Scenario.**

## 11. Discussion

435   We have presented a series of scenarios modelling hypogene carbonic acid speleogenesis (CAS), (Palmer, 2017). The aquifer is recharged by meteoric water with defined $p_{CO_2}$ that percolates through the vadose zone and feeds the water table with a solution saturated with respect to calcite. From depth water with high $p_{CO_2}$ saturated with respect to calcite intrudes into the aquifer.

At the water divide of the flow domains that are generated in Darcy flow mixing of the waters creates a mixing fringe where
440   MC causes widening of the fractures located in that zone. Statistical fluctuations may generate regions of enhanced hydraulic conductivity that attract flow focusing it into a narrow constriction. There one by one mixing is enhanced causing maximal dissolution rates. At the end of this constricted region flow is ejected to form a wide mixing zone. Provided the aquifer is sufficiently wide this process is repeated until the water exits. In heterogeneous aquifers zones of enhanced conductivity may already exist. In that case they are seeds for constrictions. This way a cave system is created with up and down dipping
445   passages as described by Palmer (2017) for the CAS caves in the black hills, South Dakota.

CAS is similar to sulfuric acid speleogenesis (SAS). In SAS, oxygen rich waters from the surface mix with water rising from the depth that is saturated with respect to calcite and contains $H_2S$. This way similar as in CAS a mixing zone is created. There by bacterial aid $H_2S$ is oxidized to $H_2SO_4$ that dissolves limestone readily thereby producing $CO_2$ as further agent for dissolution. Since there is not sufficient knowledge on details of this complex processes, especially about the location of
450   bacteria in the fractures or their junctions and the kinetics of bacterial oxidation, modelling of SAS is not possible. Nevertheless, the basic processes of cave formation should be similar to those of CAS. Therefore, albeit with care our results may serve to interpret SAS cave systems.

## 12. Conclusion

We have proposed first digital models of hypogene carbonic acid speleogenesis (CAS) as suggested already in 1989 by
455   Palmer and Palmer.They argued that where waters saturated with respect to calcite but with differing Ca-concentration are mixed mixing corrosion will become active as a cave forming mechanism. Many geological settings can be considered where such conditions are true. In this work we explore by digital modelling a simple idealized setting. Meteoric water percolates into a limestone massif attaining saturation with respect to calcite when it meets the water table. From below deep-seated water loaded with $CO_2$ rises reaches saturation with respect to calcite and invades into the limestone. In Darcy
460   flow two flow domains are established that are separated by a water divide. There, due to dispersive diffusion, the different waters mix in a fringe surrounding the water divide and mixing corrosion sets in widening the aperture of the fractures. The water leaves the aquifer at a seepage face in most of our computer runs. The cave evolves first at the output and in the depth of the aquifer close to the input from below. Between these regions a wide fringe of smaller dissolution rates develops.

465 This fringe in its middle due to the heterogeneity of the fractures develops constrictions with increasing dissolution rates and attracts flow from both waters that mix there to reach maximal dissolution rates. Finally a cave system bending up and down attracts all flow such that its pattern stays stable in time but with increasing widths of conduits.

Depending on the parameters of the computer runs such as e.g. dimensions of the aquifer, magnitude of water input, q, from below and the amount, $Q$, of meteoric precipitation as well as the ratio $Q/q$ that determines the position of the initial flow domains a variety of cave patterns are obtained. We have modeled cases when the meteoric input varies in time and found

470 that the early state of cave evolution determines its final pattern.

Our modelling results have some consequences to the definition of hypogene karst. Both definitions, that by Palmer (2000) from the geochemical view as well as that by Klimchouk (2007;2016) from a hydrological approach state independence of hypogene karstification on surface processes. In CAS as well as in SAS, however, surface processes do have a strong impact.

## 13. Author Contributions

475 WD initiated the work and wrote the text. FG is the author of the model code. He performed simulations and prepared figures. The manuscript is based on the in-depth discussions of both authors.

## 14. Competing interests

The authors declare that they have no conflict of interest.

## 15. Acknowledgments

## References

Audra, P., and Palmer, A. N.: Research frontiers in speleogenesis. Dominant processes, hydrogeological conditions and resulting cave patterns, Acta Carsologica, 44, 10.3986/ac.v44i3.1960, 2015.
Birk, S., Liedl, R., Sauter, M., and Teutsch, G.: Hydraulic boundary conditions as a controlling factor in karst genesis: A
485 numerical modeling study on artesian conduit development in gypsum, Water Resources Research, 39, art. no.-1004, 2003.
Buhmann, D., and Dreybrodt, W.: The kinetics of calcite dissolution and precipitation in geologically relevant situations of karst areas.2. Closed system, Chemical geology, 53, 109-124, 1985.
Chaudhuri, A., Rajaram, H., and Viswanathan, H.: Early-stage hypogene karstification in a mountain hydrologic system: A coupled thermohydrochemical model incorporating buoyant convection, Water Resources Research, 49, 5880-5899,
490 10.1002/wrcr.20427, 2013.
Cheung, W., and Rajaram, H.: Dissolution finger growth in variable aperture fractures: Role of the tip-region flow field, Geophysical Research Letters, 29, 32-31-32-34, 10.1029/2002gl015196, 2002.
Dreybrodt, W.: Processes in karst systems: physics, chemistry, and geology, Springer-Verlag, Berlin; New York, xii, 288 pp., 1988.

495    Dreybrodt, W.: The role of dissolution kinetics in the development of karst aquifers in limestone - A model simulation of karst evolution, Journal of Geology, 98, 639-655, 1990.

Dreybrodt, W.: Principles of early development of karst conduits under natural and man-made conditions revealed by mathematical analysis of numerical models, Water Resources Research, 32, 2923-2935, 1996.

Dreybrodt, W., Gabrovšek, F., and Romanov, D.: Processes of speleogenesis: A modeling approach, Carsologica, edited by:
500    Gabrovsek, F., Založba ZRC, Ljubljana, 375 pp., 2005.

Dreybrodt, W., and Gabrovšek, F.: Dynamics of wormhole formation in fractured limestones, Hydrol. Earth Syst. Sci., 23, 1995-2014, 10.5194/hess-23-1995-2019, 2019.

Eisenlohr, L., Meteva, K., Gabrovsek, F., and Dreybrodt, W.: The inhibiting action of intrinsic impurities in natural calcium carbonate minerals to their dissolution kinetics in aqueous $H_2O$-$CO_2$ solutions, Geochimica Et Cosmochimica Acta, 63, 989-
505    1001, 1999.

Gabrovsek, F., Romanov, D., and Dreybrodt, W.: Early karstification in a dual-fracture aquifer: the role of exchange flow between prominent fractures and a dense net of fissures, Journal of Hydrology, 299, 45-66, http://dx.doi.org/10.1016/j.jhydrol.2004.02.005, 2004.

Gabrovsek, F., and Dreybrodt, W.: Karstification in unconfined limestone aquifers by mixing of phreatic water with surface
510    water from a local input: A model, JOURNAL OF HYDROLOGY, 386, 130-141, 2010.

Gabrovšek, F., and Dreybrodt, W.: A model of the early evolution of karst aquifers in limestone in the dimensions of lenght and depth / F. Gabrovšek, W. Dreybrodt, Journal of Hydrology, str. 206-224, 2001.

Groves, C. G., and Howard, A. D.: Early development of karst systems.1. Preferential flow path enlargement under laminar-flow, Water Resources Research, 30, 2837-2846, 1994.

515    Hanna, R. B., and Rajaram, H.: Influence of aperture variability on dissolutional growth of fissures in karst formations, Water Resources Research, 34, 2843-2853, 1998.

Jeong, C. H., Kim, H. J., and Lee, S. Y.: Hydrochemistry and genesis of CO2-rich springs from Mesozoic granitoids and their adjacent rocks in South Korea, Geochemical Journal, 39, 517-530, 10.2343/geochemj.39.517, 2005.

Kaufmann, G.: Modelling unsaturated flow in an evolving karst aquifer, Journal Of Hydrology, 276, 53-70, 2003.

520    Kaufmann, G., Romanov, D., and Hiller, T.: Modeling three-dimensional karst aquifer evolution using different matrix-flow contributions, Journal of Hydrology, 388, 241-250, 2010.

Kaufmann, G., Gabrovšek, F., and Romanov, D.: Deep conduit flow in karst aquifers revisited, Water Resources Research, 50, 4821-4836, 10.1002/2014wr015314, 2014.

Kaufmann, G., and Romanov, D.: Modelling speleogenesis in soluble rocks: A case study from the Permian Zechstein
525    sequences exposed along the southern Harz Mountains and the Kyffhäuser Hills, German, Acta Carsologica, 48, 10.3986/ac.v48i2.7282, 2019.

Klimchouk, A.: Hypogene Speleogenesis: Hydrogeological and Morphogenetic Perspective, National Cave and Karst Research Institute, Special Paper National Cave and Karst Research Institute, Carlsbad, 106 pp., 2007.

Klimchouk, A., Palmer, A. N., Waele, J. D., Auler, A. S., and Audra, P.: Hypogene Karst Regions and Caves of the World,
530    in: Cave and Karst Systems of the World, edited by: LaMoreaux, J. W., Springer International Publishing, 911, 2017.

Klimchouk, A.: Chapter 114 - Speleogenesis—Hypogene, in: Encyclopedia of Caves (Third Edition), edited by: White, W. B., Culver, D. C., and Pipan, T., Academic Press, 974-988, 2019.

Klimchouk, A. B.: 6.19 Hypogene Speleogenesis, in: Treatise on Geomorphology, edited by: Shroder, J. F., Academic Press, San Diego, 220-240, 2013.

535    Klimchouk, A. B.: The Karst Paradigm: Changes, Trends and Perspectives, Acta Carsologica, 44, 10.3986/ac.v44i3.2996, 2016.

Li, S., Kang, Z., Feng, X.-T., Pan, Z., Huang, X., and Zhang, D.: Three-Dimensional Hydrochemical Model for Dissolutional Growth of Fractures in Karst Aquifers, Water Resources Research, 56, e2019WR025631, 10.1029/2019wr025631, 2020.

540    Palmer, A. N.: Origin and morphology of limestone caves, Geological Society of America Bulletin, 103, 1-21, 1991.

Palmer, A. N.: Hydrogeologic control of cave patterns, in: Speleogenesis: Evolution of karst aquifers, edited by: Klimchouk, A., Ford, D. C., Palmer, A., and Dreybrodt, W., National Speleological Society, Huntsville, 77-90, 2000.

Palmer, A. N.: Cave geology, Cave Books, Dayton, Ohio, vi, 454 p. pp., 2007.

Rajaram, H., Cheung, W., and Chaudhuri, A.: Natural analogs for improved understanding of coupled processes in
545 engineered earth systems: examples from karst system evolution, Current Science, 97, 1162-1176, 2009.

Siemers, J., and Dreybrodt, W.: Early development of karst aquifers on percolation networks of fractures in limestone, Water Resources Research, 34, 409-419, 1998.

Svensson, U., and Dreybrodt, W.: Dissolution kinetics of natural calcite minerals in $CO_2$-water systems approaching calcite equilibrium, Chemical Geology, 100, 129-145, 1992.

550 Szymczak, P., and Ladd, A. J. C.: Wormhole formation in dissolving fractures, Journal of Geophysical Research: Solid Earth, 114, n/a-n/a, https://doi.org/10.1029/2008JB006122, 2009.